Journal of Mechanical Design and Vibration, 2018, Vol. 6, No. 1, 9-16
Available online at http://pubs.sciepub.com/jmdv/6/1/2

DOI:10.12691/jmdv-6-1-2

Vibration Control of a Flexible Beam with Embedded Shape Memory Alloy Wire

Nicholas G. Garafolo*, Garrett McHugh

Department of Mechanical Engineering, The University of Akron, Akron, OH 44325, U.S.A.
*Corresponding author: nicholas.g.garafolo@uakron.edu

Abstract Structural vibrations can damage systems and lead to high cycle fatigue, excess noise or even catastrophic failure. The research presented herein aims to quantify the effect of embedded shape memory alloy (SMA) wire as an active suppression system to mitigate such vibrations in a flexible clamped-free beam. A silicone beam with embedded SMA wire was designed. Natural frequencies were calculated using a frequency response function (FRF) at varying temperatures. Experiments resulted in an average natural frequency shift of 44.7% and an amplitude decrease of 34% at the tip of the beam. Control samples were created using the same dimensions and silicone material. One control sample contained embedded aluminum wire while the other sample contained no embedded material. The addition of the unactuated SMA wire resulted in an average natural frequency shift of 160% and amplitude decrease of 44.6% while the actuated SMA wire resulted in a shift of 258% and amplitude decrease of 63.6%. The natural frequency of the embedded aluminum wire sample remained the same at low and high temperatures, leading to the conclusion that the frequency shift of the SMA sample was a result of the shape memory effect.

Keywords: *shape memory alloy, vibration control, natural frequency control, clamped-free beam*

Cite This Article: Nicholas G. Garafolo, and Garrett McHugh, "Vibration Control of a Flexible Beam with Embedded Shape Memory Alloy Wire." *Journal of Mechanical Design and Vibration*, vol. 6, no. 1 (2018): 9-16. doi: 10.12691/jmdv-6-1-2.

1. Introduction

Structural vibration experienced within mechanical systems are generally unwelcome and can be experienced in applications of numerous fields including aerospace, biomechanical, and civil engineering. Allowing continuous high amplitude vibrations can be dangerous and even result in catastrophic failure. Methods for mitigation of these vibrations are typically desired to reduce the risk of damage to the system components and optimize system performance.

Aside from energy-harvesting applications, the presence of vibration encountered in mechanical or aerospace designs are undesirable as the oscillations can create problems stemming from high cycle fatigue, excess vibration noise and permanent damage or failure of components [1]. The mild cases of these oscillations include wing flutter experienced in passenger aircraft leading to mild passenger discomfort. High-cycle fatigue in components experiencing regular vibration suffer from microfractures leading to decreased life time or even failure. In some cases, the exponential increase in vibration amplitude induced by dynamic instabilities can lead to catastrophic structural failure. The Tacoma Narrow's bridge experienced such a case in 1940 when torsional oscillations induced by aeroelastic flutter lead to the collapse of the bridge [2]. Examples of vibrations caused by dynamic instabilities can be seen in aerospace components, energy harvesting systems and even as the driving effect of oronasal snoring [3]. The presence of these vibrations must be considered in the design of any structural component.

The research presented herein seeks to investigate the ability of embedded shape memory alloy (SMA) wire to mitigate vibration in a flexible clamped-free beam through active control of embedded shape memory alloy (SMA) wire in order to alter the vibration behavior of a silicone beam. SMA is a proven "smart material" that has a depth of macroscopic and microscopic applications [4,5]. Due to its large capacity of work, there has been successful implementation of SMA ranging from actuators [6] to space applications [7].

2. Vibration Mitigation Techniques

Conventionally, systems are designed with enough spring and damper support to ensure that the structure is stable enough to avoid vibration and dynamic instabilities within the operating range of the system. Systems that are designed to resist these instabilities often come with the disadvantages of increased weight or complex and expensive components. It is therefore beneficial to create an active system that can mitigate vibration without compromising design and cost optimization.

Several mitigation techniques have been investigated including piezo-electric actuators (PZT), servohydraulic actuation and active fiber composites [8]. Surface bonded PZTs were tested by NASA Langley Research Center's

Flutter Research and Experimental Device (FRED). The experiment studied two 1.5 in. by 1 in. piezoelectric wafer actuators bonded to a ridged wing. The wing was attached to a flexible mount system designed in a wind tunnel. The flexible mount system measured plunge depth with two spring tines while pitch angle was measured with a single pitch spring. The two piezoelectric actuators were adhered to either side of the base of one of the spring tines. A 20% increase in the upwind speed required to induce flutter was observed upon activation of the PZT actuators [9]. Hydraulic actuation has been utilized in helicopter blades to induce blade torsion in order to change the blade's angle of attack and alter the vibrational properties. Studies have shown that application of these systems have reduced resonance frequencies by 20% [10]. These systems, however, where heavy and required many components. Active fiber composites have also been studied in rotor blade twist applications. The composites consisted of a laminated structure of fiberglass plies and PZT fiber plies [11]. The systems were costly to produce and were found to be difficult to activate due to poor electrical connections.

SMA materials have an advantages over piezoelectric actuators in the areas of force to weight ratio and work output. It may also be possible to create passive vibration mitigation actuators in applications involving high heat such as the blades and rotors of a turbine.

2.1. SMA Vibration Control

In the design of dynamic systems, many components can be generalized as a beam on which vibrational analyses can then be performed. Numerous studies have shown that SMA can impact the vibrational properties of beams with varying boundary conditions. A numerical analysis along with experimental validations of clamped-clamped beams with embedded pre-strained SMA wires are conducted in [15,21]. These studies revealed that above the Austenite finish temperature (A_f) the shape memory effect of the SMA material is able to alter the natural frequencies of composite beams with varying volume fraction, number of wires and pre-strain of the SMA wire by effectively increasing the overall stiffness of the beam. Experimental studies by Rezaei et al. [14] and numerical studies by Damanpack et al. [22] have both concluded that the maximum amplitude of vibrating clamped-clamped composite beams with embedded shape memory alloys can be reduced up to 66% upon actuation of the shape memory effect.

SMA wires have also been confirmed to impact the vibrational properties of clamped-free composite beams numerically and experimentally. Barzegari [23] uses an Euler-Bernoulli, Timoshenko and third-order beam theory to show numerically that the addition of actuated SMA wires can dramatically decrease natural frequencies of simply supported and clamped-clamped beams while dramatically increasing the natural frequencies of clamped-free beams. An experimental study by Nakshatharan [24] using SMA wire applied externally to a clamped-free beam with a constant excitation frequency confirmed that beam tip amplitude reduction of approximately 60% can be achieved in first bending mode. The introduction of the shape memory effect, whereby the shape memory alloy material acts as both a damper and a means of variable stiffness have been confirmed for HCF mitigation [16,17,18,19] using thin sheet metal SMA topically adhered onto a clamped-free beam. This study highlights an amplitude reduction of 92% in the second bending mode with constant excitation frequency.

SMA wires have also been confirmed to work in position tracking of vibrating beams with relatively high displacements [25]. Further investigation of position tracking with embedded SMA wires could lead to control system wherein SMA wires are able to continuously monitor the vibrational properties of a beam and apply the shape memory effect according to user preference, leading to system which can operate autonomously.

2.2. Research Objectives

The research presented quantifies the effectiveness of using embedded shape memory alloy (SMA) wire to actively change the vibration characteristics of a clamped-free flexible beam. This was accomplished through an experimental investigation of the vibratory response of a silicone beam with embedded SMA wire. The vibratory response of the beam depicts itself through changes in stiffness, amplitude, and natural frequency. The study seeks a fundamental understanding of the dynamic change that an SMA wire embedded beam undergoes as a result of the shape memory effect. The study was accomplished by the following specific tasks:

1. Designing a Mold that can shape a silicone beam with embedded SMA wire.
2. Creating the silicone beam with embedded SMA wire shaped to a single loop
3. Identifying the natural frequency of the composite system
4. Creating and programming a joule heater to control the temperature of the SMA wire
5. Investigating the system's response to varied temperature input
6. Quantifying the change in natural frequency of the silicone beam

3. Shape Memory Alloys

Shape memory alloys are defined by their ability to "remember" a set shape and transform to this shape after deformation through a solid-solid phase change. The material's ability to produce work over large areas without producing residual strains makes it a popular research topic in mechanical, medical and aeronautical fields [12]. The material starts off in a Martensite phase where it is soft and deformable. If the material is deformed, it can be forced into an Austenite phase when it is heated to an "Austenite finish temperature" A_f which will cause the material to return to its original shape. A hysteretic loop of this solid-solid phase change can be seen in Fig. 1. SMAs are able to absorb and dissipate energy through this hysteretic shape change when they are cyclically loaded. The shape changing properties of SMAs have been utilized in many applications including sensing, actuation and structural support. Embedding SMAs into a vibrating

structure will introduce the shape memory effect and dampen the structure upon actuation, thereby mitigating oscillations and leading to reduced amplitudes and increased natural frequencies.

SMAs can be found in two states depending on the sample's surrounding temperature. The low temperature state is known as Martensite and is a soft deformable state that can have a tetragonal, orthorhombic, or monoclinic crystal structure. Martensite exists in two different forms; as twinned Martensite and detwinned or "reoriented" Martensite. The high temperature state is known as Austenite and is often referred to as the "parent phase" that has a cubic crystal structure. These phases can be described with four transition temperatures. The hysteresis begins with a cooling transformation defined by the Martensitic starting temperature (M_s). As the temperature decreases, the material moves towards the Martensite finish temperature (M_f). At this temperature the material is now in the twinned Martensite phase. The material then goes through a heating transformation and moves toward the Austenitic start temperature (A_s). The cycle is concluded when the material is heated to the Austenitic finish temperature (A_f). The material can be deformed while in the twinned Martensite phase, reorienting the crystal structure and causing the material to become detwinned. If the detwinned Martensite is heated above A_f, it will reorient itself into the original parent shape the material had whilst in the twinned Martensite phase. This process and its transition temperature are depicted in Figure 1.

The SMA's phase transformation from Martensite to Austenite is an endothermic process where latent heat is produced. The reverse transformation is an exothermic process where latent heat is absorbed. The produced/absorbed latent heat can cause temperature variations through the material which can alter its behavior. If the SMA experiences an external load, thermal energy can be added to the material if the heat generated during the exothermic transformation does not fully dissipate. This adds constraints on the heating and cooling rates as well as the rate of the applied load. In tests requiring temperature variations, controllable temperature methods are required such as Joule heating or liquid baths for cooling. The required temperature variations rates for uniform material temperatures are case sensitive and must be determined experimentally [12].

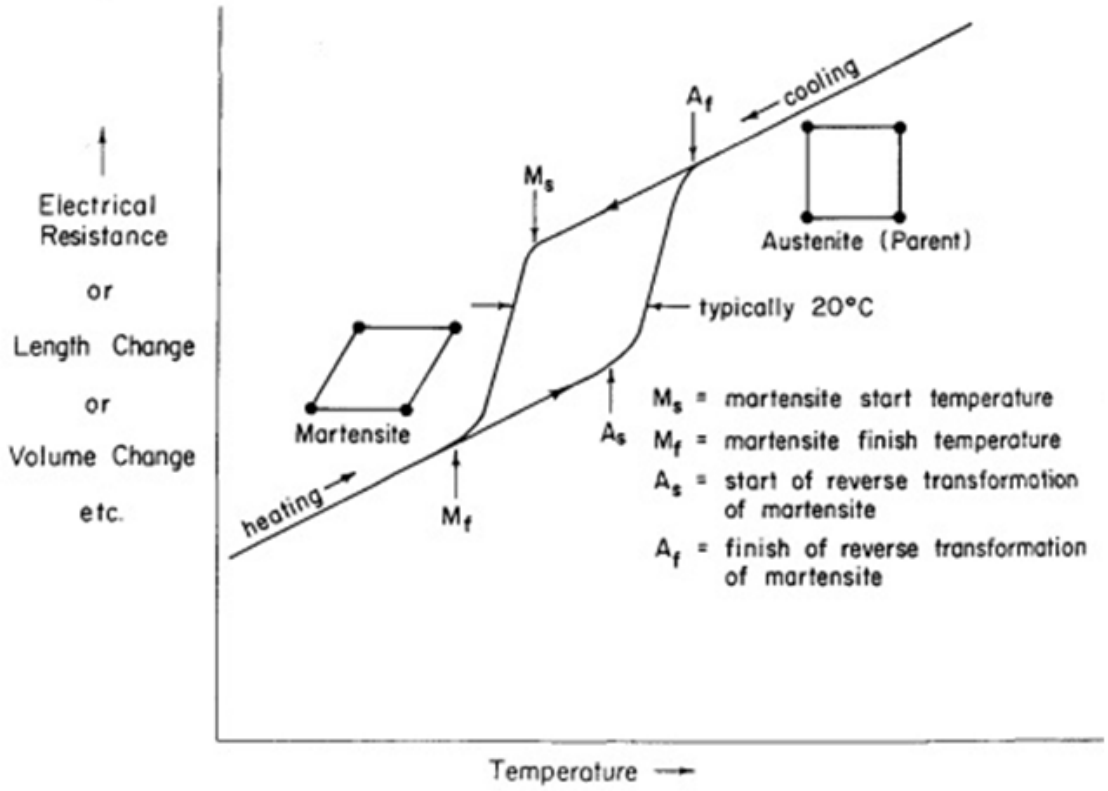

Figure 1. Theoretical plot of property change vs. temperature for the Martensite to Austenite phase transformation of a shape memory alloy [13]

4. Experimental Approach

An experiment was designed to quantify the vibratory response of a flat silicone beam with embedded SMA wire. The experiment will utilize a dynamic shaker to produce vibrations which can subsequently be studied. Control samples were also created to compare the SMA embedded beam to a beam with embedded aluminum wire along with a beam containing no embedded material. FRF frequencies were recorded and analyzed at varying beam temperatures.

4.1. Test Specimen

Experimental analysis was performed on a 1/8 in. thick, 2.5 in. by 1 in. silicone beam with embedded SMA wire. A 0.5 in. section of the beam was clamped onto the dynamic shaker leaving a test section of 2 in. by 1 in. Straight annealed, Nitinol M type wire was used which has an actuation temperature of 113°F ± 18°F and a diameter of 0.6 mm. The wire runs along the length of the beam and a single loop is made at the edge of the beam which can be seen in Figure 2. The beam was made using

a 3D printed mold and shore 25A durometer silicone. The 3D printed mold was designed so that the SMA wire could be clamped between the two halves of the silicone beam. The SMA wire was shaped into its loop and set along the center of the silicone beam during molding.

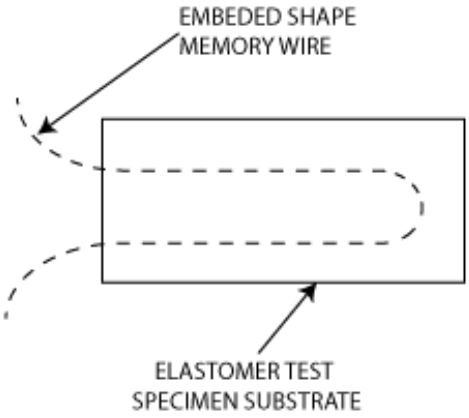

Figure 2. Silicone Beam with Embedded SMA wire Shaped into a Single Loop

Two control samples were utilized to compare with the experimental results. The first sample was made with the same silicone material as the test sample with the same geometric dimensions but excluded the embedded SMA wire. The second sample was also made with the same silicone material and geometric dimensions, but included an embedded aluminum wire of similar thickness. This sample was made as a comparison with the test sample while the SMA is in a Martensitic state. ASTM B211 aluminum wire was used with a diameter of 0.635mm. The aluminum wire has an elastic modulus of 70 GPa compared to Martensitic Nitinol's modulus of 28-40 GPa. The silicone control sample was put through the same frequency sweep test as the test sample at room temperature. The aluminum control sample was tested at room temperature and 135°F.

4.2. Experimental Setup

The silicone beam was clamped onto a dynamic shaker to act as a cantilever beam as seen in Figure 3. A 110 lb. MB RED dynamic shaker was used to perform frequency sweeps. For this test, input was created by using a signal generator. Clamps were constructed out of phenolic material to electrically isolate the beam from the dynamic shaker. A Polytec OFV 534 laser scanner was used to measure displacement at a single point on the surface of the beam. A small amount of reflective tape was placed on the surface of the beam to increase laser visibility. An accelerometer was attached to the surface of the dynamic shaker for use in FRF calculations. Joule heating was used to heat the SMA wire using a 750 Watt power supply. An infrared laser was used to measure the surface temperature of the silicone beam during testing. The infrared laser was calibrated using a hand-held infrared sensor measuring the surface of the silicone beam as it was joule heated from 75 to 110°F. A separate scan was also performed on the test specimens using a Polytec PSV-400 three dimensional scanning laser vibrometer to measure tip displacements and capture mode shapes.

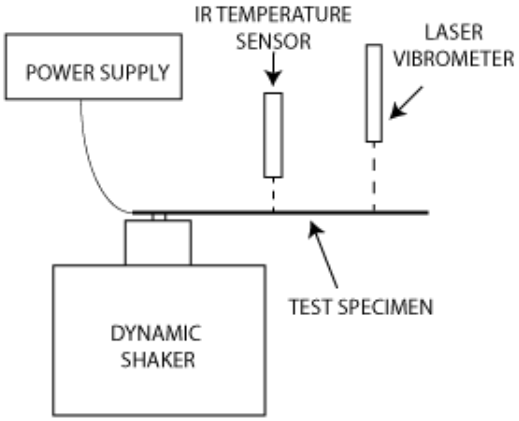

Figure 3. Experimental Test Setup of Silicone Beam with Embedded SMA Wire

4.3. Experimental Procedure

Two separate experiments were conducted in this study. Firstly, an initial test to measure first bending mode natural frequencies was performed on each silicone beam. A single point scanning laser vibrometer was utilized to gather vibrational data and resulting FRF calculations produced the natural frequency of the beam. Input frequency for FRF calculation was gathered using an accelerometer mounted to the dynamic shaker. The frequency range was set to run from 100 to 1000 Hz over a span of 2 seconds. Joule heating was used to heat the SMA wire embedded in the beam as the infrared laser measured the beam's temperature. In theory, increasing the temperature of the SMA material should activate the shape memory effect thereby increasing the stiffness of the beam. This increased temperature should result in an increase in the beam's natural frequency and shift the peak of the calculated FRF to a higher frequency. The surface temperature of the beam was recorded as the sample was put through a heating and cooling cycle. Data was recorded for every increase or decrease of 5°F. FRF results were plotted to observe any resulting hysteresis and natural frequencies were compared.

A second experiment was conducted using the Polytec PSV-400 scanning laser vibrometer to scan multiple points along the beam during vibration in order to measure beam tip displacements of the first bending mode shape. Magnaflux developer was sprayed on the surface of the test specimens to create a reflective surface for the laser to read. A frequency sweep from 0 to 400 Hz was used with 1600 FFT lines (0.25 resolution). The SMA and aluminum embedded test samples went through the same temperature sweep used in the initial experiment. The laser's on board data management software detected maximum tip displacement and mode shapes of the specimen in real time display. A 3 by 10 point mesh was used to detect vibrations over each specimen and create the two dimensional mode shape.

Preliminary testing was conducted to observe the system's natural frequency response at increasing temperatures. It was observed that the beam reached the peak of its natural frequency shift at 130°F. A temperature range of 75 to 135°F was then selected to observe any resulting hysteresis. Starting at 75°F, FRF data was recorded by the scanning laser and DAQ. The temperature was then

increased by 5°F and data recorded. This process proceeded until the sample reached 135°F. From this point, the procedure was repeated but with a decrease in temperature of 5°F increments. The experiment concluded upon return to 75°F. This procedure was run 11 times to ensure repeatability. Each time the experiment was run, all equipment was restarted and the surface of the silicone beam was cleaned with alcohol to ensure an accurate IR sensor reading.

4.4. Uncertainty of Results

Vibration data was acquired at a bandwidth of 1000 Hz with 4000 FFT lines. Uncertainty for frequency was equal to half of the resolution of the FRF giving a frequency uncertainty of ±0.125 Hz. Two dimensional laser scanning acquired data at a bandwidth of 400 Hz with 1600 FFT lines giving the same uncertainty of ±0:125 Hz. The error in the frequency response of the scanning laser vibrometer decoder was ±0.1 dB. The bias error of the scanning laser vibrometer is negligible compared to the precision error of the tests. The resolution of the laser's data acquisition system was 16 bit. The non-linearity in the shear accelerometer was less than 1%. The test was repeated eleven times on the sample giving a student t value of 2.228 for a 95% confidence window.

5. Results and Discussion

On average, the peak FRF frequency of the test sample started at 13 Hz at 75°F and increased to about 17.91 Hz at 135°F. The experiment resulted in an average overall peak FRF frequency shift of 5.82 Hz, or 44.7%. The highest peak frequency recorded was 6.75 Hz (51.9%) and the lowest was 5.25 Hz (40.38%). The peak FRF frequencies at increasing and decreasing sample temperatures for all eleven runs of this experiment were averaged and plotted in Figure 4. Values for the frequency shift along with the peak FRF frequency of each run are shown in Table 1. The repeatability of the test is displayed in Figure 5 and Figure 6. The peak frequencies of all eleven runs for increasing temperatures are shown in Figure 5 while Figure 6 shows the decreasing temperatures.

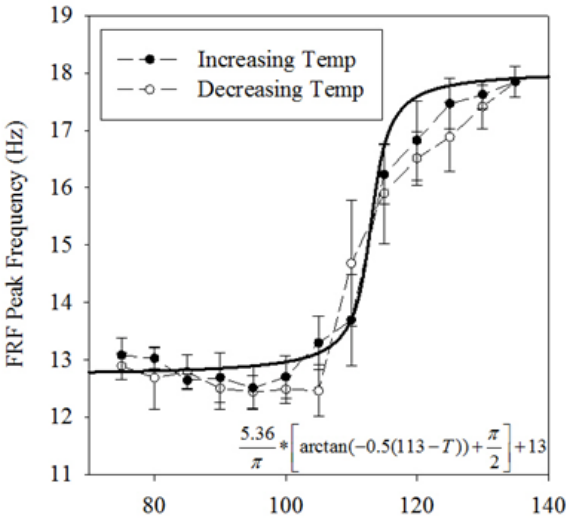

Figure 4. Graph Showing the Average Peak FRF Frequency vs. Temperature of all Eleven Runs Along with arctan Curve Fit

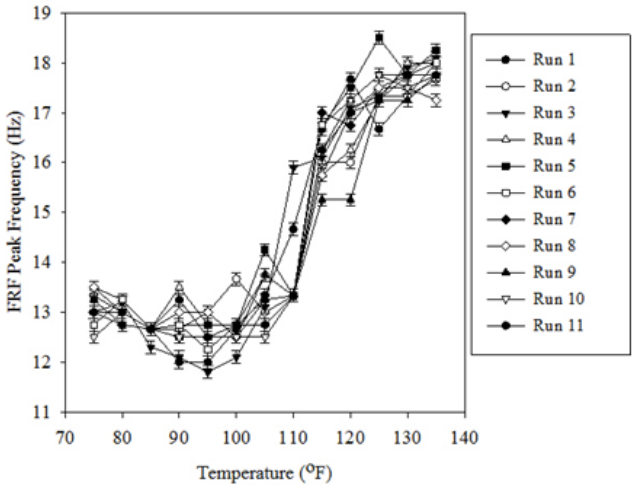

Figure 5. Graph showing Repeatability of Peak FRF Frequency vs. Temperature for Increasing Temperatures of all Eleven Runs

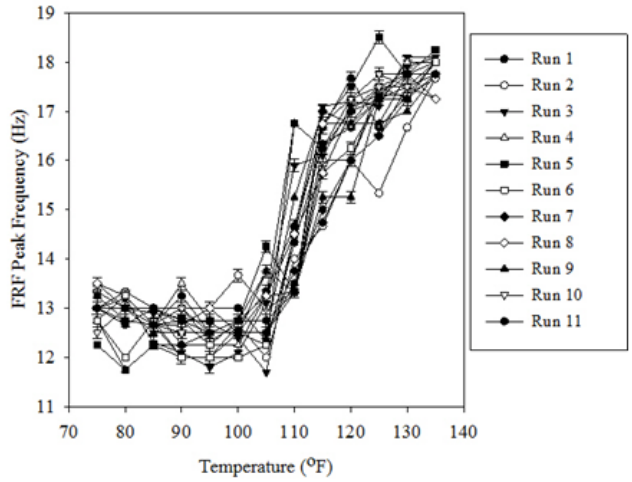

Figure 6. Graph showing Repeatability of Peak FRF Frequency vs. Temperature for Decreasing Temperatures of all Eleven Runs

Table 1. Peak FRF Natural Frequencies and Overall Frequency Shifts of all Eleven Runs.

Run	Freq. Shift (Hz)	Peak Freq. (Hz)
1	6	18
2	5.75	17.75
3	6.5	18
4	6.25	18
5	6.75	18.5
6	6	18
7	5.25	17.75
8	5.5	17.75
9	5.25	17.75
10	5.25	17.75
11	5.5	17.75
Mean (Hz)	5.82	17.91
$u_{precision}$ (Hz)	1.205	0.125

An arctan curve fit for the average of all eleven runs is displayed in Figure 4. The arctan curve was derived from the following strain-temperature equation used in [20]

$$\epsilon(T,\delta) = \frac{\epsilon_S}{\pi}\left[atan\left(\beta\left(\delta\frac{w}{2} + T_c - T\right)\right) + \frac{\pi}{2}\right] + \epsilon_0. \quad (1)$$

Table 2 defines the parameters of the equation which describes the natural frequency (ϵ) as a function of temperature (T) and a sign operator δ. The sign operator δ dictates whether the equation is for the increasing temperature or decreasing temperature of the hysteresis. Resulting data shows that the increasing and decreasing temperatures followed approximately the same paths leading to a hysteresis width (w) of zero. The average data of the runs had a root mean square deviation of 0.332 when compared to the arctan curve.

Table 2. Symbols and Definitions used in arctan Curve Fit Function

Symbol	Definition	Value
ϵ_s	Hysteresis Height	5.36 (Hz)
w	Hysteresis Width	0 (Hz)
T_c	Critical Temp. at Center of Hysteresis	113 °F
β	Slope of Hysteresis at Critical Temp.	0.5
ϵ_0	Natural Frequency at Room Temp.	13 (Hz)

The resulting two dimensional mode shapes of the vibrating samples are seen in Figure 8 – Figure 10. The figures show the first bending mode of the oscillating beams and the resulting amplitude change as sample temperatures are increased. Maximum tip displacement was measured using the scanning laser vibrometer at three node points along the tip of the beams. Values for the maximum tip displacements are displayed in Table 3. The average tip displacement of the embedded SMA sample for first bending mode was reduced from 292.5 µm to 192.1 µm at the peak temperature, a total amplitude reduction of 100.4 µm (34%). Decrease in the tip displacement amplitude and frequency of the actuated vs. unactuated SMA embedded sample is seen in a sine graph comparison in Figure 7. The addition of the unactuated SMA wire to the silicone structure results in a total amplitude decrease of 235.5 µm (44.6%) while the actuated SMA results in a decrease of 335.9 µm (63.6%). The aluminum control sample resulted in a small amplitude increase from 263.9 µm to 271.8 µm, an increase of 7.9 µm (2.98%). The amplitude decrease seen at peak temperatures of the SMA embedded beam indicates an increase in the stiffness of the structure while the amplitude increase seen in the aluminum sample indicates a very small decrease in structural stiffness.

As the temperature of the aluminum control sample increased, no frequency shift was seen and only a small tip displacement amplitude was observed. This was caused by the amount of aluminum material used, which was not high enough for the softened aluminum to impact the structural stability of the silicone beam. The volume of SMA wire used in the test sample was close to the same volume of aluminum used in the control sample. It can then be concluded that the frequency shift seen in the SMA test sample was caused by the shape memory effect. Comparison for resulting FRF plots for control samples and test sample can be seen in Figure 11 - Figure 12. A FRF plot of the test sample at 75°F and 135°F are also shown. The plain silicone control sample had a peak natural frequency at 5 Hz while the embedded aluminum sample resulted in a peak frequency of 14.75 Hz at every temperature.

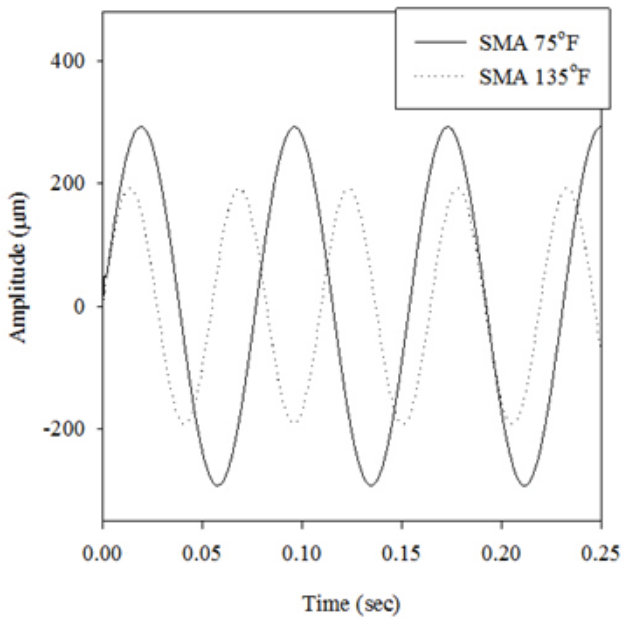

Figure 7. Maximum Tip Displacement Amplitude and Natural Frequency of Actuated and Unactuated Embedded SMA Test Sample

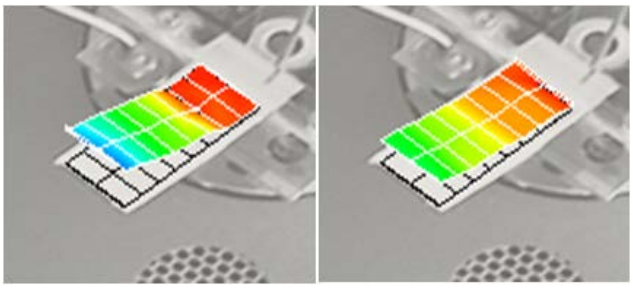

Figure 8. Mode Shape of Embedded SMA Silicone beam at 75°F (Left) and 135°F (Right)

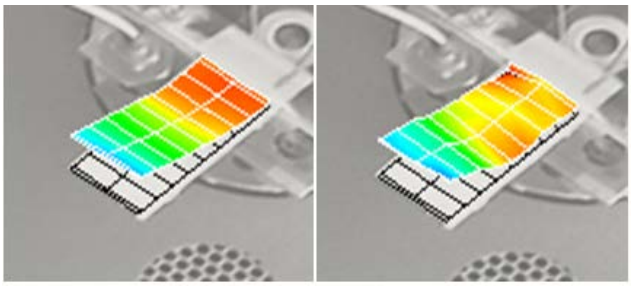

Figure 9. Mode Shape of Embedded Aluminum Silicone beam at 75°F (Left) and 135°F (Right)

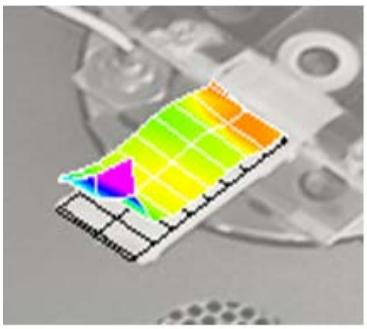

Figure 10. Mode Shape of Silicone Control Sample

Table 3. Maximum Tip Displacement of all Nodes Along the Tip of Each Sample

Sample	Node 1 (μm)	Node 2 (μm)	Node 3 (μm)	Average (μm)
Embedded SMA 75°F	285.1	276.4	316	292.5
Embedded SMA 135°F	183.6	190.3	202.3	192.1
Embedded Al 75°F	266.9	252.3	272.5	263.9
Embedded Al 135°F	274.1	257.7	286.7	271.8
Embedded SMA 75°F	777.7	417.2	389.6	528

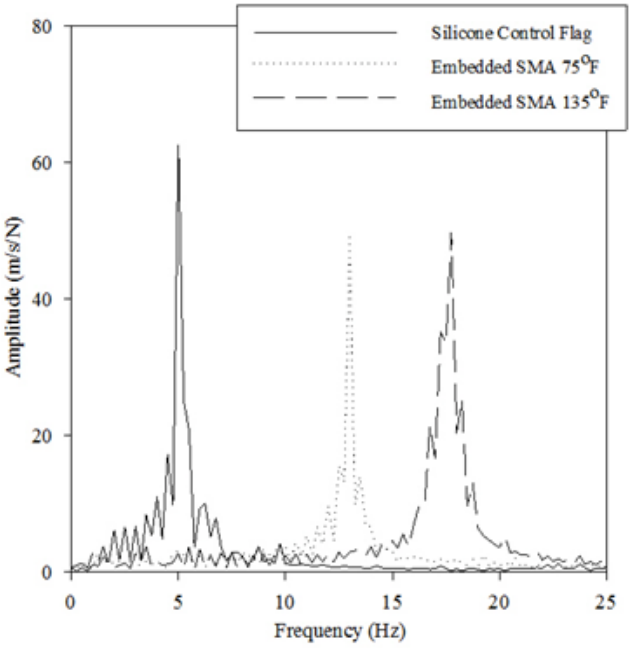

Figure 11. Mode Shape of Embedded Aluminum Silicone beam at 75°F (Left) and 135°F (Right)

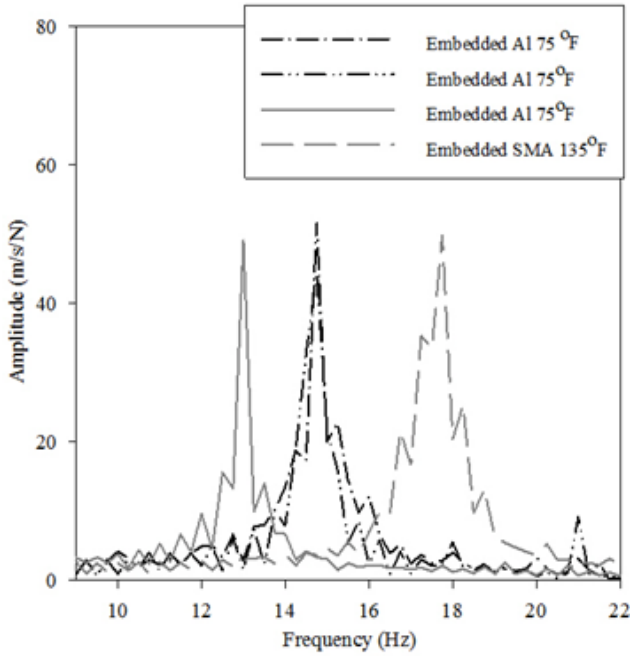

Figure 12. Mode Shape of Embedded Aluminum Silicone beam at 75°F (Left) and 135°F (Right)

Typical SMA frequency sweep testing result in data displaying a hysteretic loop similar to the one seen in Figure 1. In the test conducted, no significant hysteresis could be seen. It is suggested that this was due to the small size of the silicone beam and the amount of SMA wire used. The SMA wire was shaped into a single loop, limiting the shape memory effect and perhaps producing a hysteresis that was too small to be observed. Although no hysteresis was observed, a repeatable stiffness variation and increase in the natural frequency of the silicone beam was seen. The increase in the silicone beam's natural frequency is assumed to be analogous to an increase of the flutter actuation speed of the system. This indicates that embedded SMA wire is a feasible option for use in vibration mitigation systems.

6. Conclusions

The research presented studies the feasibility of embedded shape memory alloys (SMA) as a means for vibration control of cantilevered beams. A vibrational study was conducted on a vibrating silicone beam with embedded SMA wire. A shift in the natural frequency and tip displacement amplitude of the beam was observed upon actuation of the embedded SMA. On average, the natural frequency of the silicone beam increased from 13 Hz to 17.91 Hz, an increase of 44.7%. This increase in the natural frequency of the beam indicates an increase in the stiffness of the system. The maximum tip displacement amplitude of the flag decreased from 292.5 μm to 192.1 μm, a total reduction of 100.4 μm (34%). Reduction in vibrational amplitude of a fluttering structure could lead to safer systems that are able to operate for longer periods of time.

Comparing the actuated SMA embedded beam system to the control beam with no embedded material resulted in a frequency shift from 5Hz to 13 Hz and an amplitude shift from 528 μm to 292.5 μm. The embedded aluminum sample showed no frequency shift and a very small amplitude increase upon increased temperature. The amount of aluminum used was not enough for the softened material to significantly affect the structural properties of the silicone flag. This shows that the frequency shift and amplitude reduction observed upon the actuation of the SMA wire in the test sample was caused entirely by the shape memory effect of the embedded wire.

As a whole, the test qualified the potential an SMA actuator can have on the response of a vibrating system. The test shows that SMA's can be used in creating variable stiffness components which can be applied to numerous systems.

References

[1] G. Bir, J. Jonkman, "Aeroelastic instabilities of large offshore and onshore wind turbines", National Laboratory of the U.S. Department of Energy with the Office of Energy Efficiency and Renewable Energy (28-31 August 2007).

[2] Y. Billah, "Resonance, Tacoma narrows bridge failure, and undergraduate physics textbooks", *American Journal of Physics* 59 (2) (1990) 118-124.

[3] L. Huang, "Flutter of cantilevered beams in axial flow", *Journal of Fluids and Structures*, 9 (1) (1995) 127-147.

[4] A. Baz, K. Imam, J. McCoy, "Active vibration control of flexible beams using shape memory actuators", *Journal of Sound and Vibration*, 140 (3) (1990) 437-456.

[5] Y. Matsuzaki, "Recent research on adaptive structures and materials: Shape memory alloys and aeroelastic stability prediction", *Journal of Intelligent Material Systems and Structures* 16 (11-12) (2005) 907-917.

[6] W. Huang, "On the selection of shape memory alloys for actuators", *Materials & Design* 23 (2002) 1-19.

[7] L. M. Schetky, "Shape memory alloy applications in space systems", *Materials & Design* 12 (1991) 29-32.

[8] V. Giurgiutiu, "Review of smart-materials actuation solutions for aeroelastic and vibration control", *Journal of Intelligent Material Systems and Structures* 11 (7) (2000) 525-544.

[9] National Aeronautics and Space Administration, J. Heeg, NASA report 3241: "Analytical and experimental investigation of flutter suppression by piezoelectric actuation (1998)".

[10] P. Chen, I. Chopra, "Wind tunnel test of a smart rotor model with individual blade twist control", *SPIE* 3041 (1) (1997) 217-229.

[11] J. Rodgers, N. Hagood, "Preliminary Mach-scale hover testing of an integrated twist-actuated rotor blade", *SPIE* 3329 (1998) 291-308.

[12] P. S. Lobo, J. Almeida, L. Guerreiro, "Shape memory alloys behaviour: A review", *Procedia Engineering* 114 (2015) 776-783.

[13] C. Wayman, "Shape memory alloys", Materials Research Society (1993) 49-56.

[14] H. Rezaei, M. Kadkhodaei, H. Nahvi, "Analysis of nonlinear free vibration and damping of a clamped-clamped beam with embedded prestrained shape memory alloy wires", *Journal of Intelligent Material Systems and Structures* 23 (10) (2012) 1107-1117.

[15] K. tak Lau, L. min Zhou, X. Ming Tao, "Control of natural frequencies of a clamped-clamped composite beam with embedded shape memory alloy wires", *Composite Structures* 58 (1) (2002) 39-47.

[16] N. G. Garafolo, R.J. Collard, "Active stiffness method for high cycle fatigue mitigation using topical thin foil shape memory alloy", *Journal of Mechanical Design and Vibration*. 5 (1) (2017) 11-20.

[17] N. G. Garafolo, R.J. Collard, "Performance Mapping of an Aluminum-Nitinol Composite Vibrating Beam", *Journal of Mechanical Design and Vibration*. 5 (1) (2017) 27-36.

[18] R. Wischt, N. Garafolo, "Variable stiffness technique for turbomachinery using shape memory alloys", Proceedings from the 56th AIAA/ASCE/AHS/ASC Structures, Structural, Dynamics, and Materials Conference.

[19] R. Wischt, N. Garafolo, "The development of an active damping and stiffness technique for turbomachinery using shape memory alloys", Proceedings from the 57th AIAA/ASCE/AHS/ASC Structures, Structural, Dynamics, and Materials Conference.

[20] M. Nascimento, C. J. Araujo, L. L. de Almeida, A. Lima, "A mathematical model for the strain-temperature hysteresis of shape memory alloy actuators", *Materials and Design* 30 (3) (2009) 551-556.

[21] A. Baz, S. Poh, J. Ro and J. Gilheany, "Control of the Natural Frequencies of Nitinol-Reinforced Composite Beams", *Journal of Sound and Vibration.* 185(1), (1995) 171-185.

[22] A. R. Damanpack, M. Bodaghi, M. M. Aghdam, M. Shakeri, "On the vibration control capability of shape memory alloy composite beams. *Composite Structures.* 110 (2014) 325-334.

[23] M. M. Barzegari, M. Dardel, A. Fathi, "Vibration Analysis of a Beam with Embedded Shape Memory Alloy Wires", *Acta Mechanica Solida Sinica.* Vol. 26, No. 5, October, 2013.

[24] S. S. Nakshatharan, D. J. S. Ruth, K. Dhanalakshmi, "Design based active vibration control of a flexible structure using shape memory alloy wire actuators", Proceedings from the 6th International Conference on Sensing Technology (ICST), 2012.

[25] J. W. Sohn, Y. M. Han, S. B. Choi, "Vibration and Position Tracking Control of a Flexible Beam Using SMA Wire Actuators", *Journal of Vibration and Control*. 15(2), 263-281.